Can Azobenzene Photoisomerise When Chemisorbed on a Gold Surface?

Enrico Benassi,[1]*§ Giovanni Granucci,[2] Maurizio Persico[2] and Stefano Corni[1]

[1]*Centro S3 CNR Istituto di Nanoscienze, via G. Campi 213/a, 41125 Modena, Italy*

[2]*Dipartimento di Chimica e Chimica Industriale, Università di Pisa, via Risorgimento 35, 56126 Pisa, Italy*

* *To whom the correspondence should be addressed:*

e–mail: enrico.benassi@sns.it

phone: +39 050 509 210

fax: +39 050 563 513

§ Present address: *Scuola Normale Superiore, Piazza dei Cavalieri 7, 56126 Pisa, Italy*

Abstract

Through a combined QM/MM approach, we evaluate the photodynamics of the mono– and dithiolated azobenzenes, when they are chemisorbed on a Gold surface. The presence of the surface influences the photoisomerisation process of the chemisorbed monothiolated azobenzene. Due to steric effects, the *trans* → *cis* quantum yields decrease and the $n\pi^*$ state lifetimes become longer. The approach to the twisted conical intersection needed for the isomerisation is hindered when the molecule is attached to a substrate, because of the van der Waals interactions with the surface. For the *cis* isomer, the *cis* → *trans* photoisomerisation quantum yield is almost unaffected, since this isomer is not flat, and thus the interaction with the surface is less remarkable. Dithiolated azobenzene can photoisomerise both *trans* → *cis* and *cis* → *trans*, also when doubly linked to the surface, preserving the two bonds with the Gold atoms: The flexibility of the central azo–moiety enables the molecule to photoisomerise without any bond breaking. The quantum yields in this case are even higher than in the monothiolated case, probably because of the strained initial conformation, that must adapt to the available distances between the anchoring sites.

Keywords

Azobenzene derivatives ; Photoisomerisation ; Self–Assembled Monolayer ; Surface effects ; QM/MM approach

1. Introduction and systems description

During the last years, many efforts have been addressed to the design and the production of molecular and super–molecular reversible switchable devices.[1–14] Thanks to their reversible *trans–cis* photoisomerisation capability and the large changes of their properties after excitation, azobenzene (diphenyldiazene, 1DA) and its derivatives represent one of the most attractive classes of organic compounds for these aims.[15–25] For practical applications, the molecular switcher is usually anchored on a noble metal surface, forming Self–Assembled Monolayers (SAMs).[26–59] The surface presence affects the photoswitching behaviour, because of (i) geometric constraints imposed by the substrate or by neighbouring molecules,[45] (ii) energy delocalisation and phase relaxation within the molecule by coupling to substrate phonons, substrate electron–hole pairs, and other adsorbates,[36,52] or (iii) surface active role[51] (*e.g.* energy transfer from the molecule to the metal). These effects may hinder the switching processes,[44] but at now the mechanism comprehension is not still clarified.

Recently,[60] G. Floß *et al.* have studied the surface hopping dynamics of the *trans*–to–*cis* light–induced isomerisation of the tetra–*tert*–butyl–azobenzene (TBA) when geometrically constrained by physisorption at weakly coupling model surfaces, mimicking Au(111) and Bi(111). They simulated the non–adiabatic dynamics of *trans* TBA after excitation into the ππ* manifold around 4 eV, by a semiclassical surface hopping scheme based on semiempirical, "on the fly" quantum chemistry modified by van der Waals terms. They found clear effects due to the surface on excited–state lifetimes, in particular for the *n*π* excited state, and on quantum yields for the *trans*–to–*cis* photoisomerisation, which are lower than for free TBA by about a factor of two. They explained the de–excitation process invoking a two–step ππ* → *n*π* → S_0 mechanism. They explained the experimentally observed strong reduction of the photoisomerisation yields for TBA physisorbed on Au(111)[51] as mainly due to causes of electronic nature, *i.e.* whereas in

the free molecule the direct (intramolecular) optical electronic excitation provokes the conformational change, for the surface–bound molecules an indirect substrate–mediated process is responsible for the isomerisation.[51] Anyway, they proved that for weak physisorbtion on an electronically inactive surfaces, direct isomerisation should be still possible.

In this study we employ a similar combined Quantum Mechanical / Molecular Mechanical (QM/MM) approach to evaluate the photodynamics of the azo–derivatives, when they are chemisorbed on a Gold surface by one or two Sulphur bridges. The main objectives of this work are two: (i) to estimate the entity of the effects due to the presence of the surface on the photoisomerisation process; (ii) to find whether azobenzene is able to photoisomerise even when it is doubly anchored to the Gold surface.

In Scheme 1 the molecular systems object of the present investigation are pictured: the azobenzene ($R_1 = R_2 = H$; 1DA), the *p*–thiolated azobenzene ($R_1 = SH$, $R_2 = H$; 1DASH) and its anion ($R_1 = S^-$, $R_2 = H$; $1DAS^-$); the *p*–dithiolated azobenzene ($R_1 = R_2 = SH$; $1DA(SH)_2$) and its di–anion ($R_1 = R_2 = S^-$; $1DAS_2^{=}$). The anionic systems have been also on–top anchored at the centre of the surface of a Gold cluster (Figure 1). The $1DAS^-$ is singly anchored, while the $1DAS_2^{=}$ is doubly anchored. In the QM/MM calculations, all the species are considered neutral.

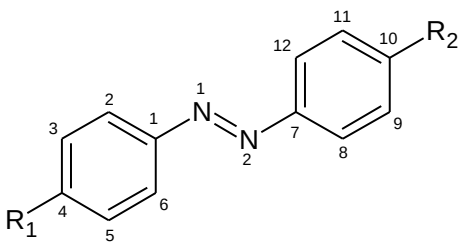

Scheme 1. Azobenzene derivatives investigated in this work ($R_{1,2} = H, SH, S^-$).

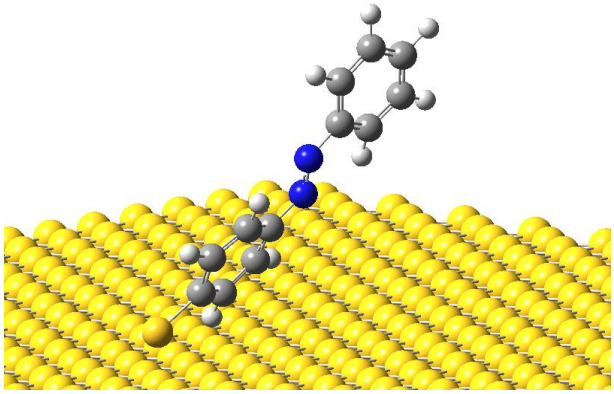

trans 1DAS@Au

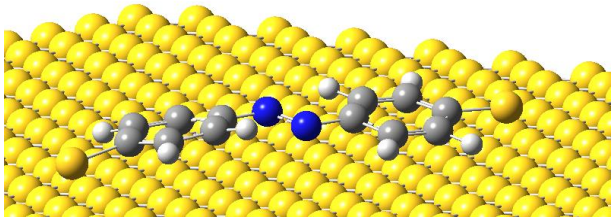

trans $1DAS_2$@Au

Figure 1. The *trans* 1DAS@Au (left) and the *trans* $1DAS_2$@Au (right).

2. Methods and computational details

From a methodological point of view, this study is structured on two levels. We first perform an investigation at (TD–)DFT level on the structural and the electronic properties of the systems pictured in Scheme 1 *in vacuo*. This investigation yields (some of) the benchmark data for subsequent steps. Next we simulate the photoisomerisation of the azo–derivatives both *in vacuo* and linked on the Gold surface. For this aim, a modified variant of the method of Persico *et al.*[61,62] for semiclassical surface–hopping dynamics[63] "on the fly" on non–adiabatically coupled potential energy surfaces is employed. This method involves the following steps:

1. Optimisation of the semiempirical parameters.
2. Initialisation of a set of trajectories on the ground state by Brownian thermal sampling.
3. Photoexcitation to the target excited electronic state, calculated from a semiempirical configuration interaction (CI) method, by sudden vertical transitions.

4. Propagation of the trajectories on coupled potentials, with gradients and non–adiabatic couplings calculated "on the fly" by the semiempirical CI method and non–adiabatic jumps governed by Tully's surface hopping algorithm.[63]

5. Post–processing calculation of the properties.

In the following, we present the computational details.

2.1 Quantum mechanical calculations on the single molecule

The molecular geometries of free R_1–1DA–R_2 ($R_{1,2}$ = H, SH, S^-; see Scheme 1), both in *trans* and in *cis* conformation, were obtained by optimisation at Density Functional Theory (DFT)[64–67] level of theory. The cc–pVTZ basis set and the Becke three–parameter Lee–Yang–Parr (B3–LYP) exchange–correlation functional[68] were employed. The properties of the first five singlet excited electronic states, the wave functions and the electronic spectra were investigated at Time Dependent DFT (TD–DFT) level of theory. In the cases of thio–derivatives, both in *trans* and in *cis* conformation, the potential energy surface was scanned as a function of the C–S bond distance. Ten points around the equilibrium geometry value were computed with relaxation of the whole geometry with exception of the scanning normal coordinate, with a scan step of 0.1 Å. The GAUSSIAN 09 computational package[69] was used for all of these calculations.

2.2 Optimisation of semiempirical parameters

The QM/MM system was set up as follows. We distinguished three sub–systems: (i) the azo–core, *viz.* the entire azobenzene, but the Sulphur atom(s), (ii) the connection atom(s) (CA(s)), *viz.* the Sulphur atom(s), and (iii) the Gold cluster. The azo–core was treated at QM level, while the Gold cluster at MM level.

The electronic energies and wave functions of the first five singlet excited states were computed on the fly by a semiempirical Configuration Interaction method based on SCF orbitals with floating occupation numbers (FOMO–CI), suited to represent reactive processes and excited states.[61] The configuration space was a CAS with six electrons in four orbitals (two lone pairs of the N atoms, a π and a π* MOs), plus all single excitations from seven occupied to six virtual orbitals (in total 94 Slater determinants). For all the QM atoms of the azo–core we adopted the semiempirical parameters already determined in a previous work.[70]

The semiempirical parameters of the connection atoms were optimised. The CA[71] is treated as an atom containing one electron only which has to reproduce the geometry and the electronic structure of the molecular environment like in a full QM calculation. The general approach to this problem is to choose a certain number of properties (geometrical data and energies) of one or more molecules which contain the same chemical environment for the CA, and find the semiempirical parameters of the connection atom which reproduce at QM/MM level the same properties. The QM/MM calculations were carried out with a development version of the MOPAC[72] semiempirical code merged with TINKER[73] and we made use of the OPLS force field. The Gold cluster was considered frozen during all the calculations. Therefore, since the azobenzene molecule does not interact with other molecules, no thermal bath is included in this model. The interaction of 1DA with the Gold atoms was described with the OPLS parameters, with additional Literature parameters for the Gold–Sulphur bond.[74] In the following, all the QM atoms in the QM/MM calculations, apart the CA's, are represented by regular or previously re–optimised AM1 parameters. The optimisation consists in the minimisation of the error function:

$$F = \sqrt{\frac{\sum_i w_i \left(d_{s,i} - d_{0,i} \right)^2}{\sum_i w_i}}$$

over all the data computed for the different structures. Here d_s are the semiempirical results, d_0 the reference data (obtained from experiment and/or high quality calculations) and w the weights.

The connection atom was characterised by a single 3*s* atomic basis function and the core charge equal to 1. The data included in the parameter optimisation were the equilibrium S–C distance, the $S_1 \leftarrow S_0$ and the $S_2 \leftarrow S_0$ transition energies, and the Potential Energy Surface (PES) ground state profile as a function of the S–C bond distance, computed at ten C–S distances, spaced by 0.1 Å, around the equilibrium geometry. These reference values were taken into account for both the *trans* and *cis* conformers of 1DASH. The corresponding reference data are those computed at (TD–)DFT level on the single molecule. Concerning the transition energies, we focused on the energy shift of the thiolated molecules with respect to 1DA. In particular, the intrusion of the σ and σ* orbitals representing the CA–C bond in the CI active space was avoided by setting the U_{ss} and β_s parameters of the connection atom to large values (–21 and –45 eV, respectively) in the SCF calculation only (whereas the subsequent CI calculation used the optimised U_{ss} and β_s).[70] During the optimisation step, the transition energies from S_0 to S_1 and to S_2 were included with two different weights (1.00 and 0.10, respectively) since in this work the target excited state is S_1.

2.3 Brownian dynamics

In order to understand and discriminate the effects due to the thio–group(s) and those due to the presence of the Gold cluster, as mentioned in Section 1, we have investigated the following systems: 1DA$(SH)_n$ *in vacuo* and 1DAS_n@Au (n = 1, 2) where the QM molecule is anchored at the centre of the Gold cluster. When we have to deal with the adsorption of thiolated molecules on Gold surface, we are faced with a long–debated issue in the Literature concerning the headgroup structure.[75] Through a remarkable joint computational and experimental study, Cossaro *et al.*[76] showed the presence of a competition between SAM ordering, driven by the lateral van der Waals interaction between alkyl chains, and disordering of interfacial Gold atoms, driven by the Sulphur–Gold interaction. The Sulphur atoms of the molecules bind at two distinct surface sites, and that of the first layer of the Gold surface contains metal atom vacancies (which are partially redistributed over different sites) as well as Gold adatoms (which are laterally bound to two Sulphur atoms). This work showed that some of the Sulphur atoms effectively occupy an atop–like position. Here we have considered a simplified structure of the adsorption, without accounting vacations nor adatoms, but preferring to assume such atop anchoring position as in the experimental picture.[77] For sake of completeness, we remark that for ideal surfaces, state–of–the–art DFT calculations[58,78–81] indicate the bridge–fcc site to be the most stable, but the atop site is not far in energy. In our model, the Gold cluster is composed of five layers of Gold atoms, forming a rectangular slab sized about (49.8 × 52.2 × 9.6) $Å^3$. The periodic boundary conditions are not applied, but the adsorbate molecule, which is approximately 12 Å long, never approaches the slab edges. The molecules were considered both in *trans*– and in *cis*–conformation. The Sulphur–Gold interaction was represented by a radial harmonic potential between each Sulphur atom and its fixed bonding site. The bonding site was identified with a Gold atom (“on top” site), but this detail in itself is of little consequence as to the overall potential energy function. The harmonic constant (k = 2.420 eV/$Å^2$) and the equilibrium distance (r_e = 2.5 Å) were obtained by fitting Literature values.[82] No additional angular potential was introduced. Thus, the Sulphur atoms are not allowed to break nor form new bonds with Gold atoms, but are constrained to the

same bonding sites along the dynamics. In the case of 1DAS$_2$@Au, the two bonding sites were chosen by considering the relaxed geometry of the molecule, that had been put on the surface with the two z(S) coordinates equal, and roto–translated until the Au–S bonds were perpendicular with respect to the surface; in such a way, the real distance available between Gold sites on the surface is respected. Therefore, the SS distance is different in case of *trans* or *cis* (12.7 or 10.1 Å, respectively). The two Gold sites chosen attempted to obtain a good compromise with respect to the SS equilibrium distance.

For each system, a single Brownian motion trajectory, using (Markovian) Langevin dynamics was run. Along this trajectory the system is subject to friction coefficients and random forces. The latter are calculated as Gaussian white noise via the second fluctuation–dissipation theorem from the assumed temperature, T. The chosen temperatures were always 300 K. In this work, we ran equilibration trajectories for 50 ps (time step δt = 0.1 fs), establishing a set of thermal initial conditions for sudden photoexcitation. Along the Brownian trajectory, the electronic spectrum was also simulated.

2.4 Surface Hopping simulations

Each Brownian trajectory was randomly sampled in order to select about 400–500 initial conditions for as many Surface Hopping trajectories. Each Brownian trajectory was randomly sampled; at each sampled geometry, a vertical excitation to S_1 was simulated on the basis of its radiative transition probability, actually selecting the sampled set according to a stochastic scheme.[83] In the end, about 400–500 sets of initial conditions were selected for each simulation. We ran simulations based on Surface Hopping with quantum decoherence corrections[84] of the *trans*–to–*cis* and the *cis*–to–*trans* photodynamics, involving the first singlet excited state. The

trajectories were stopped when one of the following conditions was met: (a) the total time reached 10 ps; or, (b) the total time exceeded 1 ps, the system reverted back to the ground state and reached a transoid or cisoid geometry (in particular, the dihedral angle CNNC is within ± 5 degrees of either 180 degrees or 0 degrees, and the CNN angles are larger than 150 degrees). All the QM/MM calculations were performed by linking MOPAC with the MM package TINKER.[73]

3. Results

3.1 Quantum mechanical calculations on the single molecule

Figure 2 collects the pictures of the geometries after DFT optimisation. For the same conformer, the geometries are quite similar to each other (see also the numerical data in Table SM.1). For the *trans* conformers, the bond and dihedral angles are not particularly affected by the presence of the Sulphur atom(s) or the thio–group(s). The selected NN (NC) bond distances show a small increase (decrease). Concerning the bond distances, this trend is appreciable also in case of the *cis* conformers, whose bond and dihedral angles also seem slightly more sensitive than those of *trans* conformers to the presence of the substituents. Anyway, in general, the presence of the Sulphur atom(s) or the thio–group(s) does not strongly affect the geometry of the ground state. This is in agreement with other Literature studies on the *p*–substituted 1DA.[85–88]

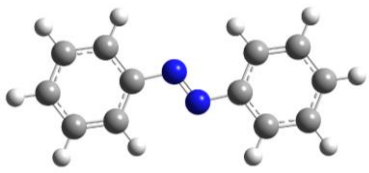

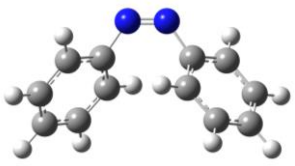

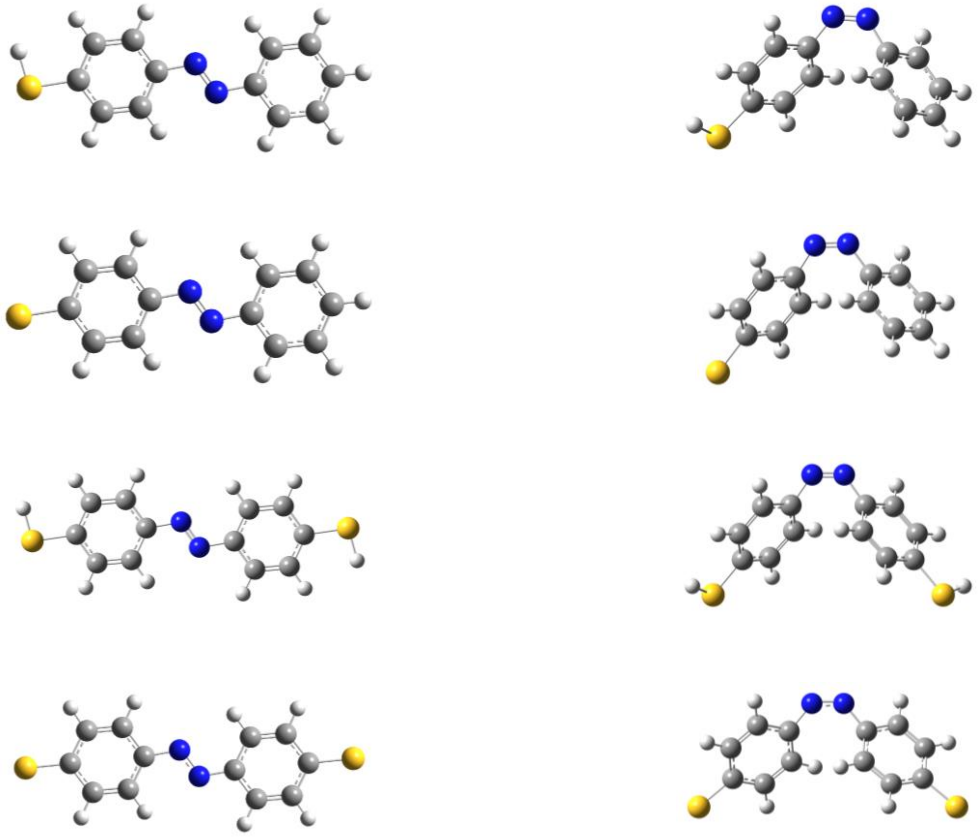

Figure 2. DFT optimised geometries, in *trans* (left) and *cis* (right) conformations.

From the TD–DFT calculations we have obtained the description of the first five singlet excited electronic states. The transition energies and oscillator strengths are collected in Table 1. The presence of one or two thio–groups causes a general increase of the oscillator strengths. With respect to the case of 1DA, the transition energies of 1DASH from S_0 to S_1 (and to S_2) are shifted by 0.0192 (–0.2827) eV for *trans* and –0.0604 (–0.4381) eV for *cis*. Further (but smaller) changes in the same directions are caused by the second substitution with a thiol group.

Table 1. Excitation energies (in eV) and oscillator strengths (in parentheses) for the $S_n \leftarrow S_0$ (n = 1 to 5) electronic transitions of the *trans* and the *cis* 1DA, 1DASH, and 1DA(SH)$_2$, as computed at TD–DFT B3LYP/cc–pVTZ level of theory.

trans	**1DA**	**1DASH**	**1DA(SH)$_2$**
1	2.5346 (0.0000)	2.5538 (0.0000)	2.5753 (0.0000)
2	3.7617 (0.7725)	3.3780 (0.8720)	3.1784 (1.1034)
3	4.1194 (0.0494)	4.0900 (0.0092)	3.8604 (0.0000)
4	4.1217 (0.0000)	4.1605 (0.0043)	4.1995 (0.0037)
5	4.9703 (0.0000)	4.2835 (0.0889)	4.2156 (0.0000)
cis	**1DA**	**1DASH**	**1DA(SH)$_2$**
1	2.5798 (0.0350)	2.5194 (0.0581)	2.4596 (0.0880)
2	4.1678 (0.0667)	3.7297 (0.1722)	3.6578 (0.2311)
3	4.2365 (0.0075)	4.1239 (0.0180)	3.6877 (0.0520)
4	4.3878 (0.0522)	4.2029 (0.0411)	4.0000 (0.0143)
5	4.4377 (0.0001)	4.3368 (0.0171)	4.2713 (0.0121)

3.2 Optimisation of semiempirical parameters

In general, concerning the geometrical parameters, the reference DFT and optimised semiempirical QM/MM results agree very well (see Table SM.1). One of the most critical aspects is the Carbon–Sulphur bond description, since it involves the QM part and the CA. In Figure 3 we show the comparison between PES scans as a function of the Carbon–Sulphur bond distance, for *trans* and *cis* conformers of 1DASH, as computed at DFT and semiempirical levels of theory. We note that the semiempirical description show a good bonding behaviour, and may be considered satisfactory in comparison with DFT calculations. From the fitting data collected in Table 2, we can obtain the minimum distance values for DFT (semiempirical) curve, *i.e.* 1.774 (1.785) Å for *trans*, and 1.776 (1.781) Å for *cis*. Thus, as a general remark, we notice that the bond distances between the connection atoms and the closest QM atom are slightly longer than the corresponding reference data. Moreover, while from DFT calculations the C–S bond length is slightly larger for the *cis* conformer than for the *trans* one, the opposite may be evinced from semiempirical calculations, where the C–S bond length is slightly larger for *trans* conformer than for *cis* one.

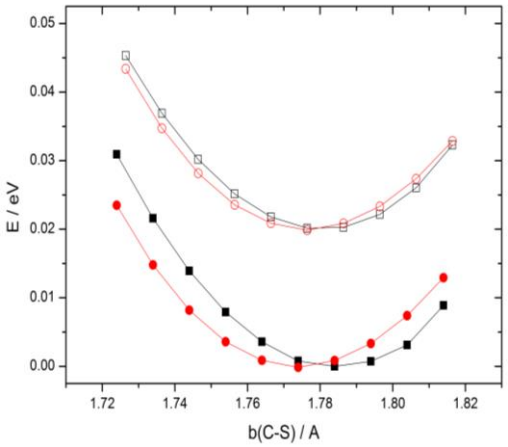

Figure 3. PES scan as a function of the Carbon–Sulphur bond distance, for *trans* (filled symbols) and *cis* (empty symbols) 1DASH, as computed at DFT (red) and semiempirical (black) levels of theory.

Table 2. Parameters for the parabolic fitting of the PES scan data shown in Figure 3.

		a_0 / eV	a_1 / eV · m^{-1}	a_2 / eV · m^{-2}	r^2
t–1DASH	DFT	27.4 ± 0.5	–30.8 ± 0.5	8.7 ± 0.2	0.99719
	semiemp.	28.1 ± 0.4	–31.5 ± 0.5	8.8 ± 0.1	0.99843
c–1DASH	DFT	27.3 ± 0.5	–30.7 ± 0.5	8.6 ± 0.2	0.99717
	semiemp.	28.2 ± 0.4	–31.7 ± 0.5	8.9 ± 0.1	0.99887

After the optimisation routine, the transition energies from S_0 to S_1 (and to S_2) are 2.8548 (4.3901) eV for *trans* and 2.8690 (4.8677) eV for *cis* 1DASH (Table 3). With respect to 1DA, the transition energies from S_0 to S_1 (and to S_2) are shifted of 0.0251 (0.0206) eV for *trans* and –0.0237 (0.0038) eV, values that have to be put in comparison with those obtained at TD–DFT, see above. The discrepancies with respect to the TD–DFT shifts are satisfactory for the transition from the ground to the $n\pi^*$ state, while they are larger (under 0.5 eV) for the transition from the ground to the $\pi\pi^*$ state. This is not surprising since during the optimisation procedure we imposed a larger weight for the first transition than for the second. In Supplementary Material, Table SM.2 reports the re–optimised semiempirical parameters.

Table 3. $S_1 \leftarrow S_0$ and $S_2 \leftarrow S_0$ transition energies (in eV) for 1DA and 1DASH, target values for 1DASH, and discrepancies.

	1DA	**1DASH**	**1DASH (target)**	**Difference**
trans				
1	2.8297	2.8548	2.8489	0.0059
2	4.3695	4.3901	3.9858	0.4043
cis				
1	2.8927	2.8690	2.8323	0.0367
2	4.8639	4.8677	4.4258	0.4419

Table 4. Distance of sulphur and nitrogen atoms from the Gold surface (in Å), from the Brownian dynamics. For the meaning of L and U labels, see the text.

	S	N1	N2
t–1DAS@Au	2.68 ± 0.06	3.47 ± 0.17 (L)	3.37 ± 0.17 (L)
		5.18 ± 0.59 (U)	5.45 ± 0.98 (U)
t–1DAS2@Au	2.68 ± 0.05	3.59 ± 0.19	3.56 ± 0.18
c–1DAS@Au	2.67 ± 0.05	5.49 ± 1.82	6.51 ± 1.90
c–1DAS2@Au	2.67 ± 0.05	5.07 ± 0.48	5.06 ± 0.48

3.3 Brownian dynamics

In Figure 4 the energies monitored along the Brownian dynamics are plotted for the system chemisorbed on the cluster (see also Figure SM.1). For *t*–1DAS@Au, the potential and the total energies sharply decrease around 12 ps of about 15 kcal/mol. This correspond to a progressive enlarging of the tilt angle, until the molecule completely lies parallel to the Gold plane. This does not surprise since we did not include any angular potential for the CA, and thus the molecule orientation changes to maximise the dispersion interaction with the Gold surface. In the following, we shall refer to these two orientations as "U" (upright) and "L" (lying). A similar phenomenon is observed for *c*–1DAS@Au. From about 20 to 30 ps the potential and the total energy decrease of about 8 kcal/mol, because the phenyl ring closest to the surface progressively reclines, lying down on the surface, under the effect of the van der Waals potentials. In Figure SM.2, we see the S@Au and the S–C bond distances along the Brownian trajectory. The values fluctuate around the equilibrium distance (about 2.7 and 1.8 Å, respectively), without any notable behaviour. In going from the U to the L orientation, the *trans* isomer is more stabilised than the *cis* one, because the former is flat and all of its atoms can lie close to the Gold surface. This is clearly apparent from the data of Table 4, where the averaged distances of Sulphur and Nitrogen atoms from the Gold surface are shown.

t–1DAS@Au *c*–1DAS@Au

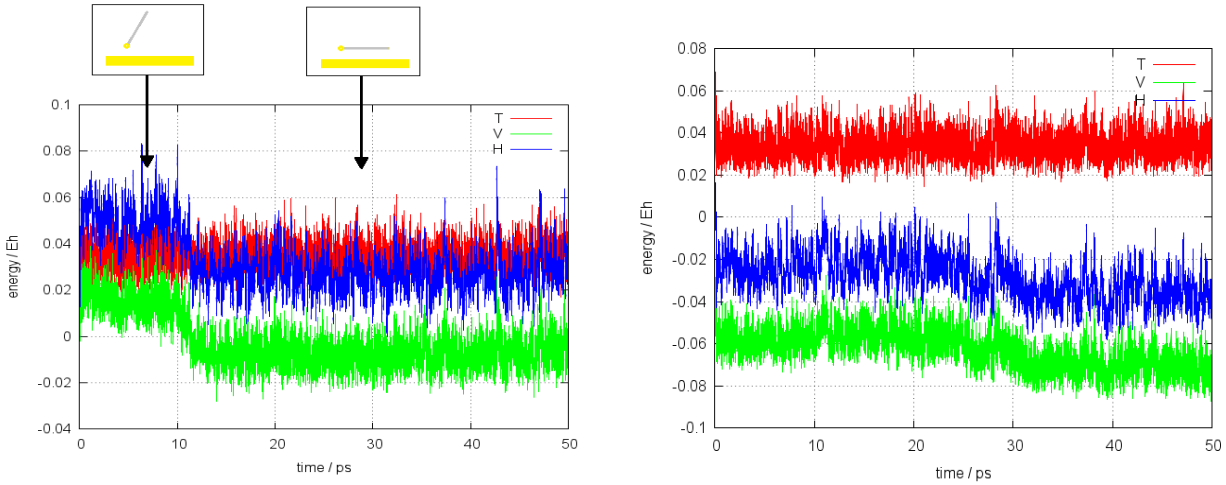

Figure 4. The kinetic (red), potential (green), and total (blue) energies monitored along the Brownian dynamics.

In Figure 5, the electronic spectra averaged along the Brownian trajectory are pictured. For *t*–1DAS@Au, the spectra are computed in three ways: (W) by averaging over the whole dynamics; (U) over the first 12 ps; and, (L) from 12 to 50 ps. The W spectrum is thus the weighted average of the U and L ones. We note that the $n \rightarrow \pi^*$ bands in the U spectrum and in free 1DASH are similar, and both stronger than in the L spectrum. This is due to the conformational freedom enjoyed by the chromophore when it is free or in the U orientation, whereas planarity is imposed in the L case. In fact, while the $n \rightarrow \pi^*$ transition is symmetry forbidden at the $\mathbf{D}_{2h}$ equilibrium geometry of azobenzene, out of plane vibrations are responsible for its (small) oscillator strength.[89] Note however that electronic interactions with the metal surface (not taken into account in this work) might have the opposite effect, by increasing the oscillator strength in the L orientation, because of the asymmetric environment in which the chromophore is placed. This is correlated with what said above concerning the molecular orientation. Even if the spectra have

broad bands, the general shape is recognisable and comparable with the TD–DFT results. For *c*–1DAS@Au, the spectrum qualitatively reproduces that computed at TD–DFT level, even if the intensity ratio between the first and the second (main) transition is smaller. The contribution of each electronic state to the spectrum is also shown. Considering the di–thiolated species, the *trans* conformer has a spectrum very similar to that of *t*–1DAS@Au sampled after 12 ps, while the *cis* differs substantially from *c*–1DAS@Au, according to the different interaction with the Gold surface (see Table 4).

t–1DASH

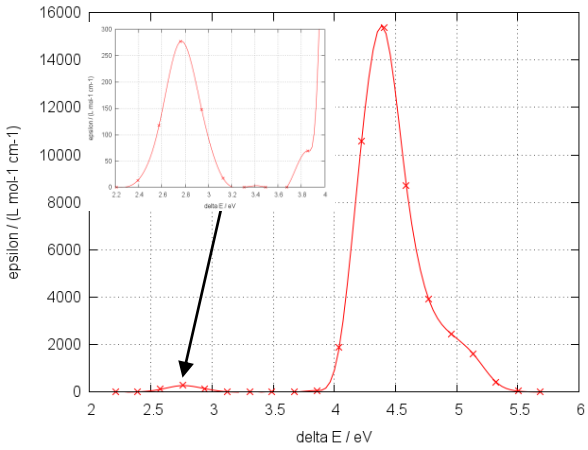

c–1DASH

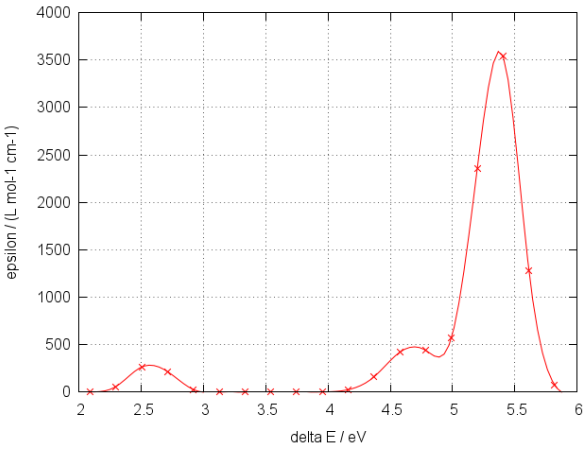

t–1DAS@Au

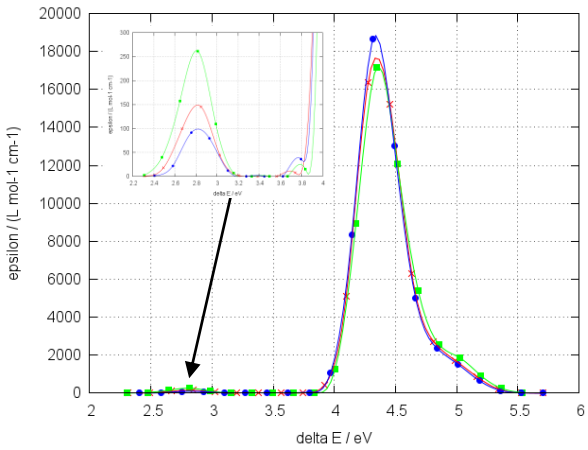

c–1DAS@Au

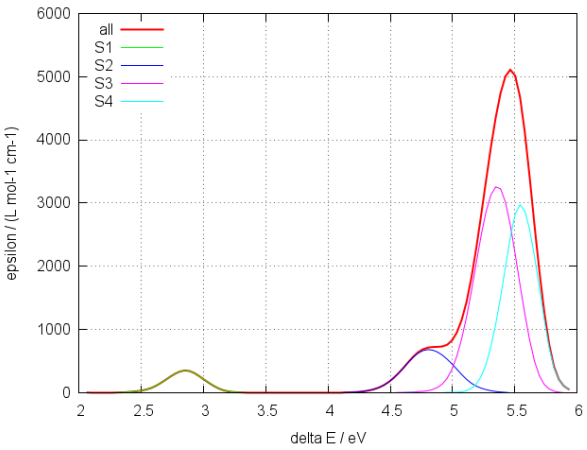

t–1DA(SH)$_2$

c–1DA(SH)$_2$

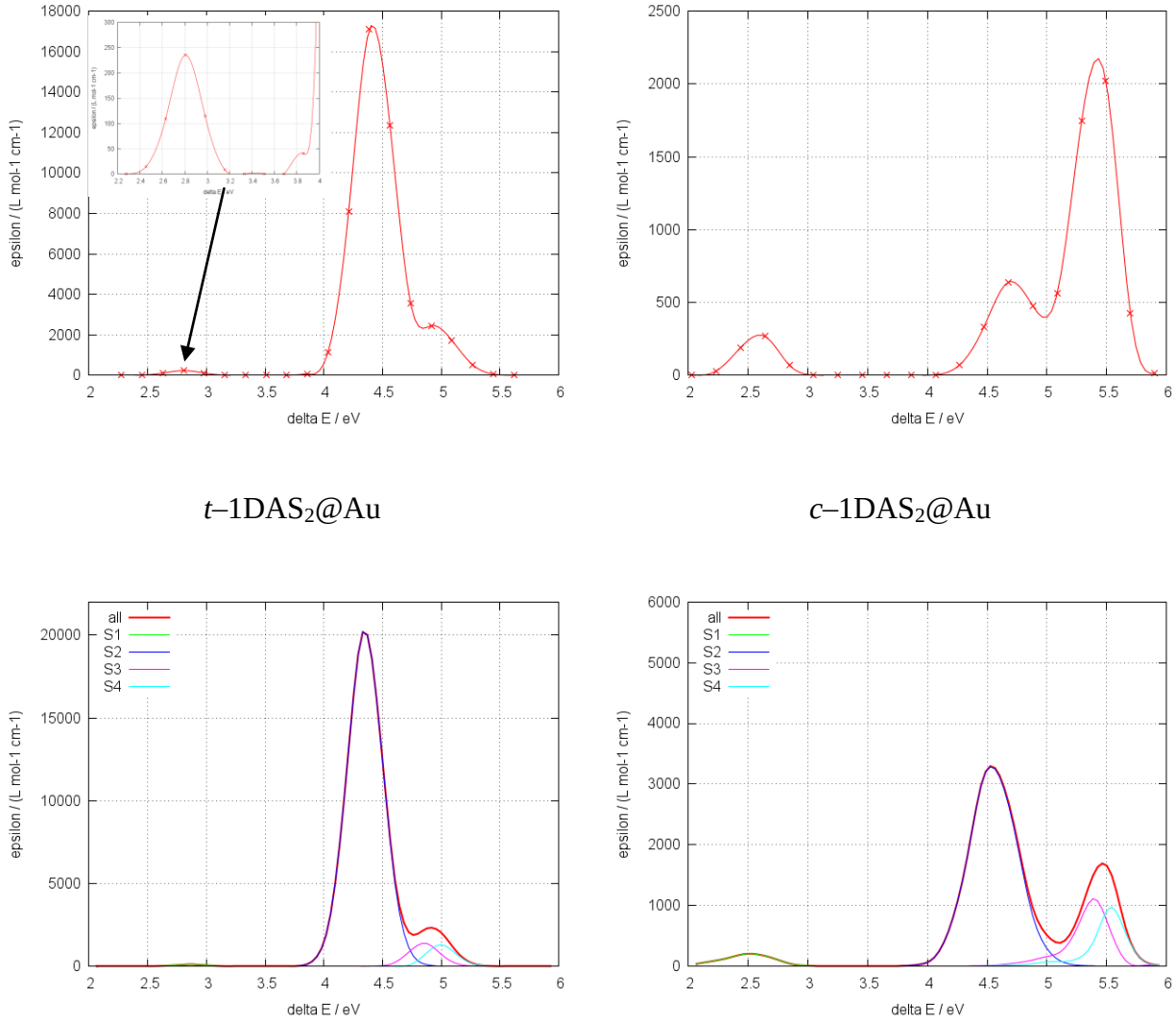

t–1DAS$_2$@Au *c*–1DAS$_2$@Au

Figure 5. Average electronic spectra along the Brownian trajectory. For *t*–1DAS@Au, the spectra are computed over the whole dynamics (red), before 12 ps (green), and after 12 ps (blue). Note the scale difference on the molar extinction coefficients.

3.4 Surface Hopping simulations

Figure 6 shows the time dependent excited state populations, that is, the fraction of trajectories running on the S_1 PES at a given time. The S_1 decay curves may be fitted by a one–exponential form $n(t) = e^{-t/\tau}$. Table 5 collects the fitted parameters. Some cases have a low number of trajectories, and therefore the values should be cautiously considered. The lifetimes are not

changed dramatically by the presence of the thio–group(s); actually, for 1DA *in vacuo*, the computed lifetimes are 0.392 ps for *trans*–to–*cis* and 0.073 for *cis*–to–*trans* (single exponential fitting of the results of ref. 89). Instead, as for the photoisomerisation quantum yields (see below), the presence of the surface affects the lifetimes. In general, we see that the lifetimes are longer than in the case of the isolated system. Instead, for TAB,[60] it was found that, passing from free–standing molecule to weak physisorption on Au(111), the lifetime for the $n\pi^*$ state becomes shorter from (0.795 ± 0.001) ps to (0.606 ± 0.003) ps at 300 K (same thermal condition as here).

For the *cis* isomer, even if the interaction with the surface lead to an increase in the S_1 lifetime, the decay remain ultrafast (well below 100 fs). For the *trans* isomer, the interaction with the gold surface play definitely a more important role, giving rise to an increase of one order of magnitude in the S_1 lifetime for *t*–1DAS@Au in the L orientation. However, quite unexpectedly, the decay time of *t*–1DAS$_2$@Au is shorter and similar to that of *t*–1DAS@Au in the U orientation. This phenomenon can be explained if we take into account that the double S–Au linkage in *t*–1DAS$_2$@Au (slightly) compresses the molecule, which is therefore in a constrained condition with a significant deviation from planarity that facilitates the S_1 state decay. This can be seen in Table 6, where we present some geometrical parameters averaged along the Brownian dynamics and for the photoisomerisation products, *viz.* the distance between the two apical Carbon atoms (d_{CC}) and between the Sulphur atoms (d_{SS}), the CNN bond angles (α_{CNN}), and the dihedral angles δ_{CNNC}. If we compare the data of the *trans* conformers, we can observe that in *t*–1DAS$_2$@Au the values of these geometrical parameters are (slightly) smaller than in *t*–1DAS@Au (L), confirming a more constraining environment for the former. Note that this is in agreement with the data of Table 4: In particular, the distances of the N atoms from the Gold surface are slightly larger for the di–thiolated molecule (which also imply a weaker van der Waals interaction with the Gold surface).

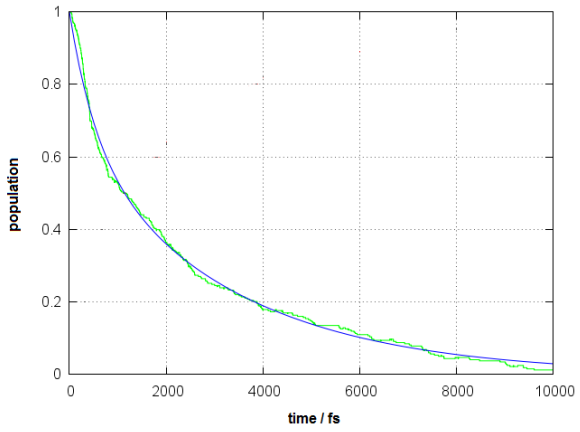

t–1DAS@Au

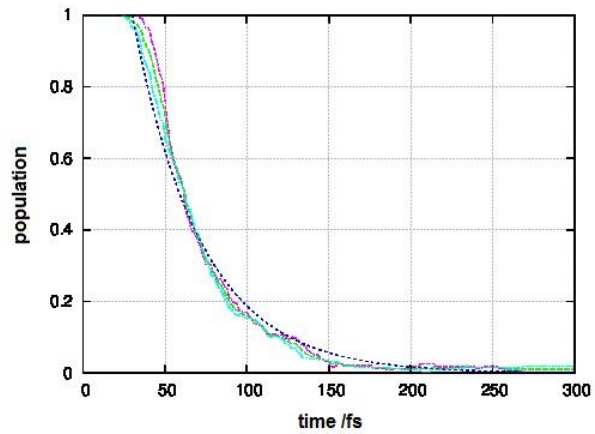

c–1DAS@Au

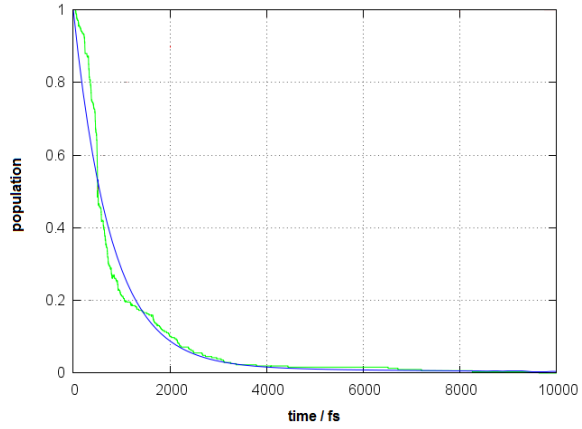

t–1DAS$_2$@Au

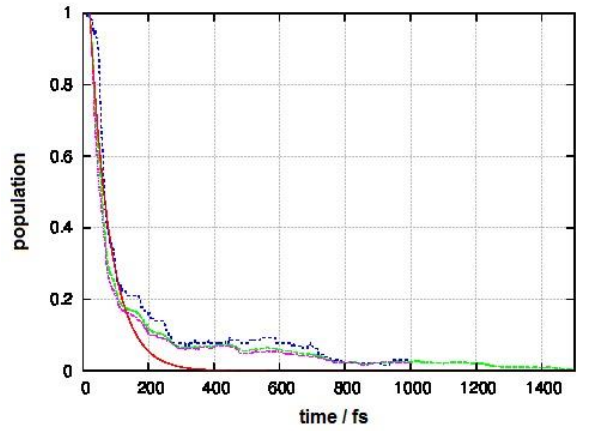

c–1DAS$_2$@Au

Figure 6. Time dependence of the S_1 state populations of *t*– and *c*–1DAS@Au, and of *t*– and *c*–1DAS$_2$@Au. The exponential fitting curve is in blue. For *t*–1DAS@Au the figure refers to the case of the trajectories coming after the first 12 ps of the Brownian motion (upright orientation).

Table 5. Total number of trajectories and quantum yields. Φ refers to *trans*–to–*cis* process or to *cis*–to–*trans* process for *t* or *c* initial conformations, respectively.

		N_{trjs}^{tot}	$\Phi \pm \Delta\Phi$
t–1DASH		275	0.43 ± 0.03
c–1DASH		303	0.59 ± 0.03
t–1DA(SH)$_2$		294	0.41 ± 0.03
c–1DA(SH)$_2$		289	0.55 ± 0.03
t–1DAS@Au	U	199	0.27 ± 0.03
	L	184	0.06 ± 0.02
c–1DAS@Au		530	0.56 ± 0.02
t–1DAS$_2$@Au		397	0.23 ± 0.02
c–1DAS$_2$@Au		588	0.83 ± 0.02

The quantum yield obtained by a simulation starting with the S_1 ($n\pi^*$) ← S_0 excitation of a given isomer is defined as the fraction of trajectories that reach the basin of equilibrium geometries of the other isomer. These trajectories will be called reactive, and the others unreactive. The computed quantum yields are listed in Table 5. The statistical standard deviations $\Delta\Phi = \sqrt{\Phi(1-\Phi)/N_{trjs}^{(tot)}}$ are also reported. For 1DA *in vacuo* $\Phi_{t\to c} = 0.33 \pm 0.02$, and $\Phi_{c\to t} = 0.57 \pm 0.02$.[90] The addition of one or two thio–groups only causes a moderate increase in $\Phi_{t\to c}$. On the contrary, the presence of the surface strongly affects the quantum yields. In the case of *t*–1DAS@Au, $\Phi_{t\to c}$ decreases considerably for the U orientation and much more for the

L one. This confirms that the presence of the surface hinders the photoisomerisation. We point out that the number of sampled trajectories of U and L *t*–1DAS@Au is similar, even if the second part of the Brownian dynamics is longer than the first part. In the case of *c*–1DAS@Au, the quantum yield is only slightly affected by the interaction with the surface.

Finally, we consider the case of the doubly bonded *t*–1DAS$_2$@Au. The computed $\Phi_{t\to c}$ is still significantly high, but almost halved with respect to 1DA(SH)$_2$ *in vacuo*. This is comparable to the dramatic decrease predicted for TBA, from $\Phi_{t\to c}$ = 0.21 to 0.12, in passing from free condition to weak physisorption on Au(111).[60] Considering the results for the S_1 decay discussed above, it is not surprising that the computed quantum yield is much larger than that obtained for *t*–1DAS@Au in L orientation. In particular, van der Waals interactions with the surface that hinder the torsion of the N=N double bond in *t*–1DAS@Au are weakened in *t*–1DAS$_2$@Au, and its starting geometry is more favourable. Figure 7 pictures the final snapshot of a reactive trajectory. In principle, the photoisomerisation of t–1DAS2@Au may proceed by two possible mechanisms: (i) either at least one of the S–Au bonds is broken when the photoisomerisation process begins, and finally, when the *cis* conformation has been reached, the molecule forms a new bond with the surface; or, (ii) the flexibility of the central azo–moiety enables the molecule to photoisomerise without any bond breaking. According to our simulations, we are enabled to say that the latter mechanism is viable, but we are not in conditions to reject the former one. In fact, in the present study, each Sulphur atom interacts harmonically with its bonding site, so neither the bond breaking nor the site to site migration can be simulated. On the other hand, the radial S–Au potential allows for a certain freedom in the sideway motion of the Sulphur atom(s). Anyway, we can say that the Au–S bond breaking mechanism is energetically less plausible. In a previous study, we computationally estimated the dissociation energy for the (mono–)thiolated 1DA anchored on–top on a (5.860 × 10.273) Å^2 Au(111) surface.[91] For the *trans* (*cis*) conformer,

D_e = 1.3116 (1.2595) eV. These values are consistent with that of the thio–benzene on a 10–atom Au(111) cluster, *i.e.* D_e = 1.935 eV, obtained though calculations performed at the *ab initio* Hartree–Fock level using a double–ζ basis set of contracted Gaussian functions including a relativistic effective core potential for Gold (LanL2DZ),[92] and with those reported in recent literature.[58,81] Even these values refer to different conditions, they seem to rule out the photoisomerisation mechanism based on the S–Au bond breaking. Moreover, we should take into account the attractive dispersion interaction between the Gold surface and the ππ* system of the 1DA, which is probably non negligible. The important element which arises from the present study is that when the azo–derivative is compressed, the photoisomerisation is favoured.

A similar pattern is also valid for the *cis* isomer, but in this case is straining (rather than compression) which favours isomerisation. In fact, *c*–1DAS$_2$@Au shows a very high photoisomerisation quantum yield: this can be explained considering that, as apparent from Table 6, *c*–1DAS$_2$@Au has larger values for d_{CC}, α_{CNN} and δ_{CNNC}. Moreover, the opening of δ_{CNNC} in the excited state dynamics is faster for *c*–1DAS$_2$@Au if compared to the mono–thiolated compound (see Figure SM.3). Note however that the rigidity of our Gold surface may lead to an artificial enhancement of these differences.

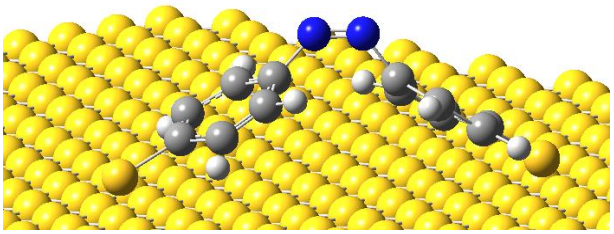

Figure 7. Final snapshot of a trajectory that gives *trans*–to–*cis* photoisomerisation of 1DAS$_2$@Au.

Table 6. Averages of some geometrical parameters along the Brownian trajectories (see main text) and for the photoisomerisation products, as obtained from the final parts of the reactive trajectories, in parentheses. For *t*–1DAS@Au data refer to the L orientation.

	d_{CC} / Å	d_{SS} / Å	α_{CNN} / degs	δ_{CNNC} / degs
t–1DAS@Au	9.05 ± 0.07	–	118 ± 3	176 ± 3
	(8.13 ± 0.92)	–	(137 ± 9)	(4 ± 1)
c–1DAS@Au	6.58 ± 0.32	–	126 ± 3	5 ± 4
	(8.87 ± 0.24)	–	(117 ± 5)	(168 ± 10)
t–1DAS$_2$@Au	8.95 ± 0.07	12.35 ± 0.09	117 ± 3	174 ± 4
	(8.09 ± 0.31)	(11.23 ± 0.41)	(136 ± 5)	(4 ± 1)
c–1DAS$_2$@Au	8.10 ± 0.14	11.32 ± 0.18	136 ± 4	7 ± 5
	(8.86 ± 0.19)	(12.15 ± 0.28)	(118 ± 6)	(168 ± 13)

From the plot of the average CNNC dihedral angle time evolution (Figure 8(a)) we see that the photoisomerisation occurs via torsion of the N=N double bond. In Figure 8(b) we have also pictured the average SS distance values $<R_{SS}>$ as a function of time, from which we can estimate the molecular length change due to the photoisomerisation. The most drastic changes in $<R_{SS}>$ occur at the same time as those of the CNNC angle. At t = 0, the SS distance of *t*–1DAS$_2$@Au is about 12 Å, whereas in the *cis* photoproduct it decreases to about 11 Å. For free *t*–1DA(SH)$_2$ the

decrease is much larger, from about 12 Å to about 9 Å. These values can be compared with those predicted at DFT level for the equilibrium geometries of *t*–1DA(SH)$_2$ and *c*–1DA(SH)$_2$ *in vacuo*, that is 12.597 and 8.868 Å. Quite clearly, while *in vacuo* the reaction product is free to approach the equilibrium geometry, the adsorbate is kept in an elongated form by the two anchoring S–Au bonds. This shows once more that the *trans*–to–*cis* photoisomerisation can occur even when the molecule is subjected to a pulling force, thanks to the elasticity of the *cis* isomer.[82]

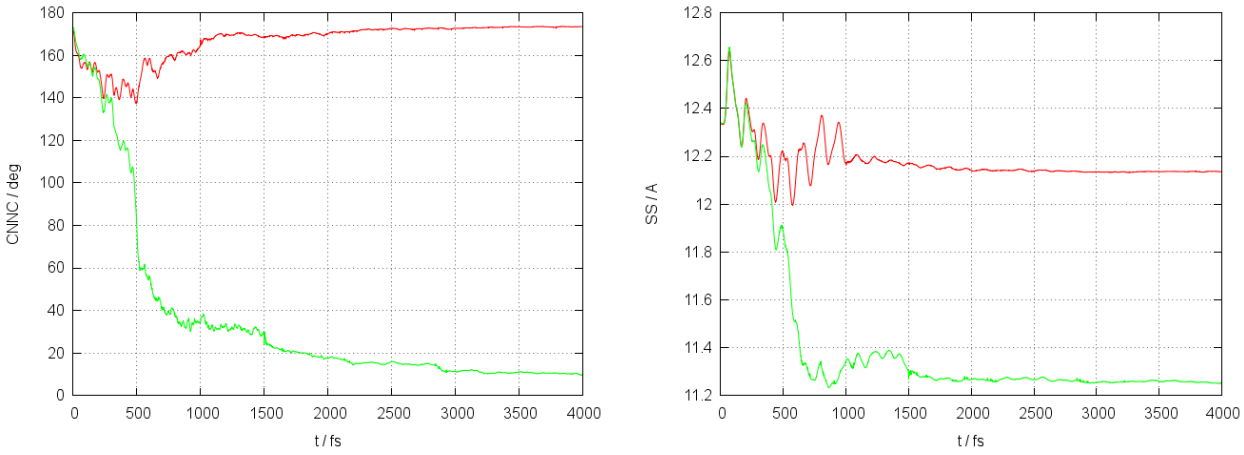

(a) (b)

Figure 8. Photodynamics of *t*–1DAS$_2$@Au. Time evolution of the average values of the CNNC dihedral angle (a) and the SS distance (b). Legend of colours: red, unreactive trajectories; green, reactive trajectories.

Table 7. Exponential lifetimes and weights obtained by fitting the S_1 state populations as a function of time.

	τ / ps

t–1DASH	[a]		0.314 ± 0.003
c–1DASH	[a]		0.0292 ± 0.0007
t–1DA$(SH)_2$	[a]		0.301 ± 0.003
c–1DA$(SH)_2$	[a]		0.0289 ± 0.0007
t–1DAS@Au	*t** → *c*	U	0.663 ± 0.002
		L	3.596 ± 0.003
	*t** → *t*	U	0.723 ± 0.002
		L	2.476 ± 0.006
c–1DAS@Au	[a]		0.0418 ± 0.0002
t–1DAS_2@Au	*t** → *c*		0.771 ± 0.004
	*t** → *t*		0.657 ± 0.008
c–1DAS_2@Au	[a]		0.0618 ± 0.0007

[a] Both *reactive* and *unreactive* trajectories have been considered together of the analysis.

4. Conclusions and further work

In this study we employ a combined QM/MM approach to evaluate the photodynamics of the mono– and dithiolated azobenzenes, when they are chemisorbed on a Gold surface. The geometrical and spectroscopical properties are satisfactorily reproduced both at (TD–)DFT and

(CI) semiempirical level. Concerning the initial prompting motivations of the present investigation, the following main conclusions can be reached:

- The presence of the surface influences the photoisomerisation process of the chemisorbed monothiolated azobenzene. The *trans*–to–*cis* quantum yields decrease and the $n\pi^*$ state lifetimes become longer, as observed for azobenzene at the centre of a solvent cluster,[70] or when tetra–*tert*–butyl–azobenzene is physisorbed over a weakly interacting surface.[60] This may be explained on the basis of purely steric effects. The approach to the twisted conical intersection needed for the isomerisation is hindered when the molecule is attached to a substrate, because the van der Waals interactions with the surface obstruct the free motion of the molecule. For the *cis* isomer, which is not flat, the interaction with the surface is less favourable, and in fact the *cis* → *trans* photoisomerisation quantum yield is almost unaffected.

- Dithiolated azobenzene can photoisomerise both ways (*trans* → *cis* and *cis* → *trans*) also when doubly linked to the surface, preserving the two bonds with the Gold atoms, since the flexibility of the central azo–moiety enables the molecule to photoisomerise without any bond breaking. The quantum yields are even higher than in the monothiolated case, probably because of the strained initial conformation, that must adapt to the available distances between the anchoring sites. The Sulphur–Gold bonds are represented by harmonic potentials, thus we are not in conditions to reject alternative mechanisms based on the migration of a Sulphur atom to another bonding site, with or without bond breaking.

In this study a number of effects that may affect the excited state lifetimes are omitted, for example: (i) The excited state quenching due to energy transfer to the metal, with electron

promotion to the conduction band (this aspect has been object of another investigation[93] the life–where time in Azobenzene molecule is shown much faster than the time of excitation energy transfer); (ii) The spin–orbit–coupling enabling an inter–system–crossing to triplet states; (iii) The vibration–phonon coupling, which is expected to proceed on a nanosecond timescale and is here neglected because in our model the Gold atoms are frozen; (iv) Finally, the possible influence of the surface electronic degrees of freedom on the existence and nature of the S_1/S_0 conical intersection, which could be investigated by cluster and/or continuum methods. Concerning the dithiolated azobenzene, the introduction of an anharmonical potential for the description of the Sulphur–Gold bond might provide significant clues about the viability of the hypothetical mechanisms of bond breaking–reforming.

Our next goal will be to describe and model the direct light switching of more molecules when densely–packed on a surface. The QM/MM approach could be used for the study of an ensemble of photoswitchable azo–derivatives in SAMs, in order to try to provide a possible answer to the important question as to whether switching is hindered by sterical restrictions or electronic coupling between the photoactive adsorbed molecules, and hopefully might help to identify those conditions under which the collective photoswitching is allowed.

Acknowledgments

We acknowledge computational time and support from CINECA under the ISCRA initiative. Funding from EU NanoSciE+ project under the Transnational grant Maecenas is gratefully acknowledged. We thank Prof. M. A. Rampi for useful discussions.

Supporting Information Available

The following Supporting Information is available: Some of the geometrical parameters of the *trans* and *cis* optimised structures calculated at DFT level; Optimised semiempirical parameters for Carbon, Nitrogen and Sulphur; The kinetic, potential, and total energies properties monitored along the Brownian dynamics; The S@Au and S–C bond distances monitored along the Brownian dynamics; Excited state dynamics of *c*–1DAS@Au and *c*–1DAS$_2$@Au. This information is available free of charge via the Internet at http://pubs.acs.org.

References and notes

[1] Griffiths, J. Photochemistry of Azobenzene and its Derivatives. *Chem. Soc. Rev.* **1972**, *1*, 481–493.

[2] Ikeda, T.; Tsutsumi, O. Optical Switching and Image Storage by Means of Azobenzene Liquid–Crystal Films. *Science* **1995**, *268*, 1873−1875.

[3] Koumura, N.; Zijlstra, R. W. J.; Van Delden, R. A.; Harada, N.; Feringa, B. L. Light–Driven Monodirectional Molecular Rotor. *Nature* **1999**, *401*, 152−155.

[4] Tamai, N.; Miyasaka, H. Ultrafast Dynamics of Photochromic Systems. *Chem. Rev.* **2000**, *100*, 1875−1890.

[5] Joachim, C.; Gimzewski, J. K.; Aviram, A. Electronics using hybrid–molecular and mono–molecular devices. *Nature* **2000**, *408*, 541–548.

[6] Feringa, B. L. *Molecular Switches*, Wiley–VCH: Weinheim, **2001**.

[7] Nitzan, A.; Ratner, M. A. Electron Transport in Molecular Wire Junctions. *Science* **2003**, *300*, 1384–1389.

[8] Balzani, V.; Venturi, M.; Credi, A. *Molecular Devices and Machines: A Journey into the Nanoworld*, Wiley: Weinheim, **2004**.

[9] Badjić, J. D.; Balzani, V.; Credi, A.; Silvi, S.; Stoddart, J. F. A Molecular Elevator. *Science* **2004**, *303*, 1845−1849.

[10] Bernà, J.; Leigh, D. A.; Lubomska, M.; Mendoza, S. M.; Pérez, E. M.; Rudolf, P.; Teobaldi, G.; Zerbetto, F. Macroscopic Transport by Synthetic Molecular Machines. *Nat. Mater.* **2005**, *4*, 704−710.

[11] Eelkema, R.; Pollard, M. M.; Vicario, J.; Katsonis, N.; Ramon, B. S.; Bastiaansen, C. W. M.; Broer, D. J.; Feringa, B. L. Nanomotor Rotates Microscale Objects. *Nature* **2006**, *440*, 163−163.

[12] Browne, W. R.; Feringa, B. L. Making molecular machines work. *Nat. Nanotechnol.* **2006**, *1*, 25–35.

[13] Klajn, R.; Stoddart, J. F.; Grzybowski, B. A. Nanoparticles functionalised with reversible molecular and supramolecular switches. *Chem. Soc. Rev.* **2010**, *39*, 2203–2237.

[14] Russew, M. M.; Hecht, S. Photoswitches: From Molecules to Materials. *Adv. Mater.* **2010**, *22*, 3348–3360.

[15] Shultz, T.; Quenneville, J.; Levine, B.; Toniolo, A.; Martinez, T. J.; Lochbrunner, S.; Schmitt, M.; Shaffer, J. P.; Zgierski, M. Z.; Stolow, A. Mechanism and Dynamics of Azobenzene Photoisomerization. *J. Am. Chem. Soc.* **2003**, *125*, 8098–8099.

[16] Kay, E. R.; Leigh, D. A.; Zerbetto, F. Synthetic Molecular Motors and Mechanical Machines. *Angew. Chem.* **2007**, *119*, 72−191; *Angew. Chem., Int. Ed.* **2007**, *46*, 72−191.

[17] Böckmann, M.; Peter, C.; Delle Site, L.; Doltsinis, N. L.; Kremer, K.; Marx, D. Atomistic Force Field for Azobenzene Compounds Adapted for QM/MM Simulations with Applications to Liquids and Liquid Crystals. *J. Chem. Theory Comput.* **2007**, *3*, 1789–1802.

[18] Puntoriero, F.; Bergamini, G.; Ceroni, P.; Balzani, V.; Vögtle, F. A Fluorescent Guest Encapsulated by a Photoreactive Azobenzene Dendrimer. *New J. Chem.* **2008**, *32*, 401−406.

[19] Siewertsen, R.; Neumann, H.; Buchheim–Stehn, B.; Herges, R.; Näther, C.; Renth, F.; Temps, F. Highly Efficient Reversible Z−E Photoisomerization of a Bridged Azobenzene with Visible Light through Resolved $S_1(n\pi^*)$ Absorption Bands. *J. Am. Chem. Soc.* **2009**, *131*, 15594−15595.

[20] Uno, S.; Dohno, C.; Bittermann, H.; Malinovskii, V. L.; Häner, R.; Nakatani, K. A Light–Driven Supramolecular Optical Switch. *Angew. Chem.* **2009**, *121*, 7498−7501; *Angew. Chem., Int. Ed.* **2009**, *48*, 7362−7365.

[21] Chen, J.; Serizawa, T.; Komiyama, M. Peptides Recognize Photoresponsive Targets. *Angew. Chem.* **2009**, *121*, 2961−2964; *Angew. Chem., Int. Ed.* **2009**, *48*, 2917−2920.

[22] Oka, Y.; Tamaoki, N. Structure of Silver(I) Complex Prepared from Azobenzenonaphthalenophane, Photochemical Coordination Change of Silver(I) and Silver(I)–Induced Acceleration of Z−E Thermal Isomerization of Azobenzene Unit. *Inorg. Chem.* **2010**, *49*, 4765−4767.

[23] Liu, M.; Yan, X.; Hu, M.; Chen, X.; Zhang, M.; Zheng, B.; Hu, X.; Shao, S.; Huang, F. Photoresponsive Host−Guest Systems Based on a New Azobenzene–Containing Crytpand. *Org. Lett.* **2010**, *12*, 2558−2561.

[24] Han, J.; Yan, D.; Shi, W.; Ma, J.; Yan, H.; Wei, M.; Evans, D. G.; Duan, X. Layer–by–Layer Ultrathin Films of Azobenzene–Containing Polymer/Layered Double Hydroxides with Reversible Photoresponsive Behavior. *J. Phys. Chem. B* **2010**, *114*, 5678−5685.

[25] Tiberio, G.; Muccioli, L.; Berardi, R.; Zannoni, C. How Does the Trans–Cis Photoisomerization of Azobenzene Take Place in Organic Solvents? *ChemPhysChem* **2010**, *11*, 1018−1028.

[26] Nagele, T.; Hoche, R.; Zinth, W.; Wachtveitl, J. Femtosecond Photoisomerization of Cis–Azobenzene. *Chem. Phys. Lett.* **1997**, *272*, 489–495.

[27] Yu, H.; Shao, H.; Luo, Y.; Zhang, H.; Liu, Z. Evaluation of the Tunneling Constant for Long Range Electron Transfer in Azobenzene Self–Assembled Monolayers on Gold. *Langmuir* **1997**, *13*, 5774−5778.

[28] Archut, A.; Vögtle, F.; De Cola, L.; Azzellini, G. C.; Balzani, V.; Ramanujam, P. S.; Berg, R. H. Azobenzene–Functionalized Cascade Molecules: Photoswitchable Supramolecular Systems. *Chem.–Eur. J.* **1998**, *4*, 699–706.

[29] Dol, G. C.; Tsuda, K.; Weener, J. W.; Bartels, M. J.; Asavei, T.; Gensch, T.; Hofkens, J.; Latterini, L.; Schenning, A. P. H. J.; Meijer B. W. *et al.* Merging of Hard Spheres by Phototriggered Micromanipulation. *Angew. Chem., Int. Ed.* **2001**, *40*, 1710–1714.

[30] Chaumet, P. C.; Rahmani, A.; Nieto–Vesperinas, M. Optical Trapping and Manipulation of Nano–Objects with an Apertureless Probe. *Phys. Rev. Lett.* **2002**, *88*, 123601−123604.

[31] Hsieh, S.; Meltzer, S.; Wang, C. R. C.; Requicha, A. A. G.; Thompson, M. E.; Koel, B. E. Imaging and Manipulation of Gold Nanorods with an Atomic Force Microscope. *J. Phys. Chem. B* **2002**, *106*, 231−234.

[32] Hugel, T.; Holland, N. B.; Cattani, A.; Moroder, L.; Seitz, M.; Gaub, H. E. Single–Molecule Optomechanical Cycle. *Science* **2002**, *296*, 1103–1106.

[33] Advincula, R.; Park, M. K.; Baba, A.; Kaneko, F. Photoalignment in Ultrathin Films of a Layer–by–Layer Deposited Water–Soluble Azobenzene Dye. *Langmuir* **2003**, *19*, 654–665.

[34] Santer, S.; Rühe, J. Motion of nano–objects on polymer brushes. *Polymer* **2004**, *45*, 8279−8297.

[35] Tian, H.; Yang, S. Recent progresses on diarylethene based photochromic switches. *Chem. Soc. Rev.* **2004**, *33*, 85–97.

[36] Moresco, F.; Meyer, G.; Rieder, K.–H.; Tang, H.; Gourdon, A.; Joachim, C. Conformational Changes of Single Molecules Induced by Scanning Tunneling Microscopy Manipulation: A Route to Molecular Switching. *Phys. Rev. Lett.* **2001**, *86*, 672–675.

[37] Jiang, W. H.; Wang, G. J.; He, Y. N.; Wang, X. G.; An, Y. L.; Song, Y. L.; Jiang, L. Photo–Switched Wettability on an Electrostatic Self–Assembly Azobenzene Monolayer. *Chem. Commun.* **2005**, 3550–3552.

[38] Kirakosian, A.; Comstock, M. J.; Cho, J.; Crommie M. F. Molecular Commensurability with a Surface Reconstruction: STM Study of Azobenzene on Au(111). *Phys. Rev. B* **2005**, 71, 113409.

[39] Choi, B.−Y.; Kahng, S. J.; Kim, S.; Kim, H.; Kim, H. W.; Song, Y. J.; Ihm, J.; Kuk, Y. Conformational Molecular Switch of the Azobenzene Molecule: A Scanning Tunneling Microscopy Study. *Phys. Rev. Lett.* **2006**, **96,** 156106.

[40] Katsonis, N.; Vicario, J.; Kudernac, T.; Visser, J.; Pollard, M. M.; Feringa, B. L. Self–Organized Monolayer of meso–Tetradodecylporphyrin Coordinated to Au(111). *J. Am. Chem. Soc.* **2006**, *128*, 15537–15541.

[41] Lim, H. S.; Han, J. T.; Kwak, D.; Jin, M. H.; Cho, K. Photoreversibly Switchable Superhydrophobic Surface with Erasable and Rewritable Pattern. *J. Am. Chem. Soc.* **2006**, *128*, 14458–14459.

[42] Katsonis, N.; Lubomska, M.; Pollard, M. M.; Feringa, B. L.; Rudolf, P. Synthetic light–activated molecular switches and motors on surfaces. *Prog. Surf. Sci.* **2007**, *82*, 407–434.

[43] Schäfer, L. V.; Muller, E. M.; Gaub, H. E.; Grubmuller, H. Elastic Properties of Photoswitchable Azobenzene Polymers from Molecular Dynamics Simulations. *Angew. Chem., Int. Ed.* **2007**, *46*, 2232–2237.

[44] Comstock, M. J.; Levy, N.; Kirakosian, A.; Cho, J.; Lauterwasser, F.; Harvey, J. H.; Strubbe, D. A.; Fréchet, J. M. J.; Trauner, D.; Louie, S. G.; *et al.* Reversible Photomechanical Switching of Individual Engineered Molecules at a Metallic Surface. *Phys. Rev. Lett.* **2007**, *99*, 038301–0338304.

[45] Pace, G.; Ferri, V.; Grave, C.; Elbing, M.; Zharnikov, M.; Mayor, M.; Rampi, M. A.; Samorì, P. Cooperative Light–Induced Molecular Movements of Highly Ordered Azobenzene Self–Assembled Monolayers. *Proc. Nat. Acad. Sci.* **2007**, *104*, 9937−9942.

[46] Morgenstern, K. Isomerization Reactions on Single Adsorbed Molecules. *Acc. Chem. Res.* **2008**, *42*, 213–223.

[47] Ferri, V.; Elbing, M.; Pace, G.; Dickey, M. D.; Zharnikov, M.; Samorì, P.; Mayor, M.; Rampi, M. A. Light–Powered Electrical Switch Based on Cargo–Lifting Azobenzene Monolayers. *Angew. Chem., Int. Ed.* **2008**, *47*, 3407−3049.

[48] Elbing, M.; Błaszczyk, A.; von Hänisch, C.; Mayor, M.; Ferri, V.; Grave, C.; Rampi, M.; Pace, G.; Samorì, P.; Shaporenko, A. *et al.* Single Component Self–Assembled Monolayers of Aromatic Azo–Biphenyl: Influence of the Packing Tightness on the SAM Structure and Light–Induced Molecular Movements. *Adv. Funct. Mater.* **2008**, *18*, 2972−2983.

[49] Qune, L. F. N. A.; Akiyama, H.; Nagahiro, T.; Tamada, K.; Wee, A. T. S. Reversible Work Function Changes Induced by Photoisomerization of Asymmetric Azobenzene Dithiol Self–Assembled Monolayers on Gold. *Appl. Phys. Lett.* **2008**, *93*, 083109.

[50] McNellis, E. R.; Meyer, J.; Reuter, K. Azobenzene at coinage metal surfaces: Role of dispersive van der Waals interactions. *Phys. Rev. B* **2009**, *80*, 205414–205424.

[51] Wolf , M.; Tegeder, P. Reversible molecular switching at a metal surface: A case study of tetra–tert–butyl–azobenzene on Au(1 1 1). *Surf. Sci.* **2009**, *603*, 1506–1517.

[52] Gahl, C.; Schmidt, R.; Brete, D.; McNellis, E. R.; Freyer, W.; Carley, R.; Reuter, K.; Weinelt, M. Structure and Excitonic Coupling in Self–Assembled Monolayers of Azobenzene–Functionalized Alkanethiols. *J. Am. Chem. Soc.* **2010**, *132*, 1831–1838.

[53] Schmidt, R.; Hagen, S.; Brete, D.; Carley, R.; Gahl, C.; Dokić, J.; Saalfrank, P.; Hecht, S.; Tegeder, P.; Weinelt, M. On the electronic and geometrical structure of the trans– and cis–isomer of tetra–tert–butyl–azobenzene on Au(111). *Phys. Chem. Chem. Phys.* **2010**, *12*, 4488–4497.

[54] Karpe, S.; Ocafrain, M.; Smaali, K.; Lenfant, S.; Vuillaume, D.; Blanchard, P.; Roncali, J. Oligothiophene–Derivatized Azobenzene as Immobilized Photoswitchable Conjugated Systems. *Chem. Commun.* **2010**, *46*, 3657–3659.

[55] Bléger, D.; Ciesielski, A.; Samorì, P.; Hecht, S. Photoswitching Vertically Oriented Azobenzene Self–Assembled Monolayers at the Solid–Liquid Interface. *Chem. Eur. J.* **2010**, *16*, 14256–14260.

[56] Crivillers, N.; Orgiu, E.; Reinders, F.; Mayor, M.; Samorì, P. Optical Modulation of the Charge Injection in an Organic Field−Effect Transistor Based on Photochromic Self−Assembled−Monolayer−Functionalized Electrodes. *Adv. Mater.* **2011**, *23*, 1447–1452.

[57] Crivillers, N.; Liscio, A.; Di Stasio, F.; Van Dyck, C.; Osella, S.; Cornil, D.; Mian, S.; Lazzerini, G. M.; Fenwick, O.; Orgiu, E. *et al.* Photoinduced Work Function Changes by Isomerization of a Densely Packed Azobenzene–Based SAM on Au: a Joint Experimental and Theoretical Study. *Phys. Chem. Chem. Phys.*, **2011**, *13*, 14302–14310.

[58] Wen, J.; Tian, Z.; Ma, J. Light− and Electric−Field−Induced Switching of Thiolated Azobenzene Self−Assembled Monolayer. *J. Phys. Chem. C* **2013**, *117*, 19934−19944.

[59] Tian, Z.; Wen, J.; Ma, J. Reactive Molecular Dynamics Simulations of Switching Processes of Azobenzene−Based Monolayer on Surface. *J. Chem. Phys.* **2013**, *139*, 014706.

[60] Floß, G.; Granucci, G.; Saalfrank P. Surface hopping dynamics of direct trans → cis photoswitching of an azobenzene derivative in constrained adsorbate geometries. *J. Chem. Phys.* **2012**, *137*, 234701.

[61] Granucci, G.; Persico, M.; Toniolo, A. Direct semiclassical simulation of photochemical processes with semiempirical wave functions. *J. Chem. Phys.* **2001**, *114*, 10608.

[62] Ciminelli, C.; Granucci, G.; Persico, M. The Photoisomerization Mechanism of Azobenzene: A Semiclassical Simulation of Nonadiabatic Dynamics. *Chem.–Eur. J.* **2004**, *10*, 2327–2341.

[63] Tully, J. C. Molecular dynamics with electronic transitions. *J. Chem. Phys.* **1990**, *93*, 1061.

[64] Hohenberg, P.; Kohn, W. Inhomogeneous Electron Gas. *Phys. Rev.* **1964**, *136*, B864–B871.

[65] Kohn, W.; Sham, L. J. Self–Consistent Equations Including Exchange and Correlation Effects. *Phys. Rev.* **1965**, *140*, A1133–A1138.

[66] Salahub, D. R.; Zerner, M. C. (Eds.) *The Challenge of d and f Electrons*; ACS: Washington, D.C., **1989**.

[67] Parr, R. G.; Yang, W. *Density–functional theory of atoms and molecules*; Oxford University Press: Oxford, **1989**.

[68] Becke, A. D. Density–Functional Thermochemistry. III. The Role of Exact Exchange. *J. Chem. Phys.* **1993**, *98*, 5648–5652.

[69] Frisch, M. J.; Trucks, G. W.; Schlegel, H. B.; Scuseria, G. E.; Robb, M. A.; Cheeseman, J. R.; Scalmani, G.; Barone, V.; Mennucci, B.; Petersson, G. A., *et al. Gaussian 09, Revision D.01*; Gaussian, Inc., Wallingford CT, **2013**.

[70] Cusati, T.; Granucci, G.; Martínez–Núñez, E.; Martini, F.; Persico, M.; Vázquez, S. Semiempirical Hamiltonian for Simulation of Azobenzene Photochemistry. *J. Phys. Chem. A* **2012**, *116*, 98–110.

[71] Toniolo, A.; Ciminelli, C.; Granucci, G.; Laino, T.; Persico, M. QM/MM connection atoms for the multistate treatment of organic and biological molecules. *Theoret. Chem. Acc.* **2004**, *93*, 270–279.

[72] Stewart, J. J. P. *MOPAC*; Fujitsu Limited, Tokyo, Japan, **2002**.

[73] Ponder, J. W. *TINKER* 6.1; Washington University School of Medicine: St. Louis, MO: 2012. http://dasher.wustl.edu/tinker.

[74] Bizzarri, A. R.; Costantini, G.; Cannistraro, S. MD simulation of a plastocyanin mutant adsorbed onto a gold surface. *Biophys. Chem.* **2003**, *106*, 111–123.

[75] Schreiber, F. Structure and Growth of Self–Assembling Monolayers. *Prog. Surf. Sci.* **2000**, *65*, 151−256.

[76] Cossaro, A.; Mazzarello, R.; Rousseau, R.; Casalis, L.; Verdini, A.; Kohlmeyer, A.; Floreano, L.; Scandolo, S.; Morgante, A.; Klein, M. L. *et al.* X–ray Diffraction and Computation Yield the Structure of Alkanethiols on Gold(111). *Science* **2008**, *321*, 943–946.

[77] Kondoh, H.; Iwasaki, M.; Shimada, T.; Amemiya, K.; Yokoyama, T.; Ohta, T.; Shimomura, M.; Kono, S. Adsorption of Thiolates to Singly Coordinated Sites on Au(111) Evidenced by Photoelectron Diffraction. *Phys. Rev. Lett.* **2003**, *90*, 066102–066106.

[78] Hayashi, T.; Morikawa, Y.; Nozoye, H. Adsorption State of Dimethyl Disulfide on Au(111): Evidence for Adsorption as Thiolate at the Bridge Site. *J. Chem. Phys.* **2001**, *114*, 7615–7621.

[79] Vargas, M. C.; Giannozzi, P.; Selloni, A.; Scoles, G. Coverage–Dependent Adsorption of CH_3S and $(CH_3S)_2$ on Au(111): a Density Functional Theory Study. *J. Phys. Chem. B* **2001**, *105*, 9509–9513.

[80] Gottschalck, J.; Hammer, B. A Density Functional Theory Study of the Adsorption of Sulfur, Mercapto, and Methylthiolate on Au(111). *J. Chem. Phys.* **2002**, *116*, 784–790.

[81] Wen, J.; Ma, J. Modulating Morphology of Thiol−Based Monolayers in Honeycomb Hydrogen−Bonded Nanoporous Templates on the Au(111) Surface: Simulations with the Modified Force Field. *J. Phys. Chem. C* **2012**, *116*, 8523−8534.

[82] Johansson, Å.; Stafström, S. Interactions between molecular wires and a gold surface. *Chem. Phys. Lett.* **2000**, *322*, 301–306.

[83] Creatini, L.; Cusati, T.; Granucci, G.; Persico, M. Photodynamics of azobenzene in a hindering environment. *Chem. Phys.* **2007**, *347*, 492–502.

[84] Granucci, G.; Persico, M. Critical appraisal of the fewest switches algorithm for surface hopping. *J. Chem. Phys.* **2007**, *126*, 134114.

[85] Wang, L.; Wang X. Ab initio study of photoisomerization mechanisms of push–pull p,p′–disubstituted azobenzene derivatives on S1 excited state. *J. Mol. Struct: THEOCHEM* **2007**, *847*,1–9.

[86] 罗世霞 (Luō, S. X.); 张笑一 (Zhāng, X. Y.); 张思亭 (Zhāng, S. T.); 朱淮武 (Zhū, H. W.); 胡继伟 (Hú, J. W.); 卫钢 (Wèi, G.) 巯基偶氮苯单分子电子传输的取代基效应 (Influence of Substituents on Electron Transport through the Single–Molecule Mercapto–Azobenzene). 物理化学学报 (*Acta Phys.–Chim. Sin.*) **2008**, *24*, 1471–1476 (written in Chinese).

[87] Jacquemin, D.; Perpète, E. A.; Scuseria, G. E.; Ciofini, I.; Adamo, C. Extensive TD–DFT investigation of the first electronic transition in substituted azobenzenes. *Chem. Phys. Lett.* **2008**, *465*, 226–229.

[88] Wang, L.; Xu, J.; Zhou, H.; Yi, C.; Xu, W. Cis–trans isomerization mechanism of 4–aminoazobenzene in the S_0 and S_1 states: A CASSCF and DFT study. *J. Photochem. Photobiol. A* **2009**, *205*, 104–108.

[89] Cusati, T.; Granucci, G.; Persico, M.; Spighi, G. Oscillator strength and polarization of the forbidden $n \rightarrow \pi^*$ band of trans–azobenzene: a computational study. *J. Chem. Phys.* **2008**, *128*, 194312.

[90] Cusati, T.; Granucci, G.; Persico, M. Photodynamics and Time–Resolved Fluorescence of Azobenzene in Solution: A Mixed Quantum–Classical Simulation. *J. Am. Chem. Soc.* **2011**, *133*, 5109–5129.

[91] Benassi, E.; Corni, S. Work Function Changes of Azo–Derivatives Adsorbed on a Gold Surface. *Submitted*. The data were obtained through plane–waves DFT calculations using the PW91 exchange–correlation functional.

[92] This value was obtained by fitting the data of ref. 19 with a function like Morse's potential. The other parameters are $a = 0.81683$ Å^{-1} and $r_e = 2.48748$ Å.

[93] Benassi, E.; Corni, S. On the Quenching of the Photoisomerisation of Azobenzene Self–Assembled Monolayers by the Metal Substrate. *J. Phys. Chem. C* **2014**, *accepted*.

Table of Contents (TOC) Image

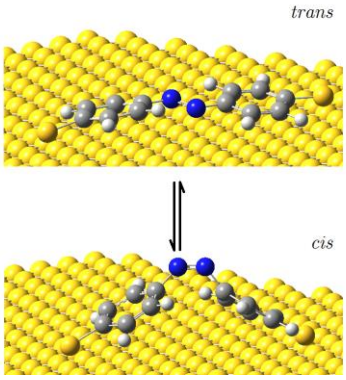

Supplementary Material

Can Azobenzene Photoisomerise When Chemisorbed on a Gold Surface?

Enrico Benassi,[1]*[§] Giovanni Granucci,[2] Maurizio Persico[2] and Stefano Corni[1]

[1]*Centro S3 CNR Istituto di Nanoscienze, via G. Campi 213/a, 41125 Modena, Italy*

[2]*Dipartimento di Chimica e Chimica Industriale, Università di Pisa, via Risorgimento 35, 56126 Pisa, Italy*

* *To whom the correspondence should be addressed:*

e–mail: enrico.benassi@sns.it

phone: +39 050 509 210

fax: +39 050 563 513

[§] Present address: *Scuola Normale Superiore, Piazza dei Cavalieri 7, 56126 Pisa, Italy*

Table SM.1. Some of the geometrical parameters of the *trans* and *cis* optimised structures calculated at DFT level. Atoms labels refer to Scheme 1. Bond distances (*b*) in Å, bond angles (α) in degrees, and dihedral angles (δ) in degrees.

trans conformers

	R_1 =	H	SH	S^-	SH	S^-
	R_2 =	H	H	H	SH	S^-
***b*(N1,N2)**		1.24840	1.25037	1.27790	1.25229	1.26848
***b*(N1,C1)**		1.41717	1.41102	1.36911	1.41002	1.39778
***b*(N2,C7)**		1.41717	1.41579	1.40046	1.41002	1.39778
***b*(C3,R_1)**		1.08185	1.77397	1.70964	1.77420	1.73964
***b*(C10,R_2)**		1.08185	1.08184	1.08256	1.77420	1.73964
α(C1,N1,N2)		115.468	115.536	117.398	115.530	116.469
α(N1,N2,C7)		115.468	115.477	114.386	115.530	116.469
δ(C1,N1,N2,C7)		179.956	179.997	180.000	179.975	180.000
δ(C2,C1,N1,N2)		179.997	179.994	180.000	180.000	180.000
δ(N1,N2,C7,C8)		179.997	179.991	180.000	180.000	180.000

cis conformers

	R_1 =	H	SH	S^-	SH	S^-
	R_2 =	H	H	H	SH	S^-
***b*(N1,N2)**		1.23887	1.24046	1.26626	1.24180	1.26498
***b*(N1,C1)**		1.43294	1.42941	1.38556	1.42855	1.41033
***b*(N2,C7)**		1.43294	1.43161	1.41134	1.42855	1.41033
***b*(C3,R_1)**		1.08148	1.77643	1.71168	1.77669	1.73933
***b*(C10,R_2)**		1.08148	1.08143	1.08215	1.77669	1.73933
α(C1,N1,N2)		124.219	124.518	127.040	124.487	128.556
α(N1,N2,C7)		124.219	124.379	125.993	124.487	128.556
δ(C1,N1,N2,C7)		9.352	10.088	15.864	10.925	16.066
δ(C2,C1,N1,N2)		136.777	142.903	168.147	141.213	161.678
δ(N1,N2,C7,C8)		136.777	135.788	134.927	141.213	161.678

Table SM.2. Optimised semiempirical parameters for Carbon, Nitrogen and Sulphur. For the parameters labels, see MOPAC User's Manual.

Parameter	**C**	**N**	**S**
USS	–49.5362424932	–68.3880615395	–21.0000000000
UPP	–33.7229206876	–56.0450179744	
UST			–13.2579459804
BETAS	–38.0000000000	–11.0187093522	–45.0000000000
BETAP	–35.0000000000	–19.5919417815	
BETST	–13.7975775576		–7.3551231371
BETPT	–10.1132638074		
ZS	1.4123765311	2.1698702072	0.9337166119
ZP	1.7492657606	1.9170209752	
ALP	2.6261992594	2.9472860000	1.2083089788
GSS	12.4926899324	16.6676533738	11.2083170638
GSP	11.5717012318	11.4705302420	
GPP	12.0176130644	13.3393080579	
GP2	7.9235319729	10.2422036244	
HSP	2.7392112908	1.7943424682	
FN11		0.0252510000	–0.2960000000
FN12		0.0289530000	0.0418000000
FN13		–0.0058060000	–0.3199000000
FN21		5.0000000000	4.5893000000
FN22		5.0000000000	5.0154000000
FN23		2.0000000000	5.1846000000
FN31		1.5000000000	1.8983000000
FN32		2.1000000000	1.2828000000
FN33		2.4000000000	1.8274000000
FN14			0.0372000000
FN24			4.9292000000
FN34			2.8804000000
PQNS	2	2	3

t–1DAS$_2$@Au *c*–1DAS$_2$@Au

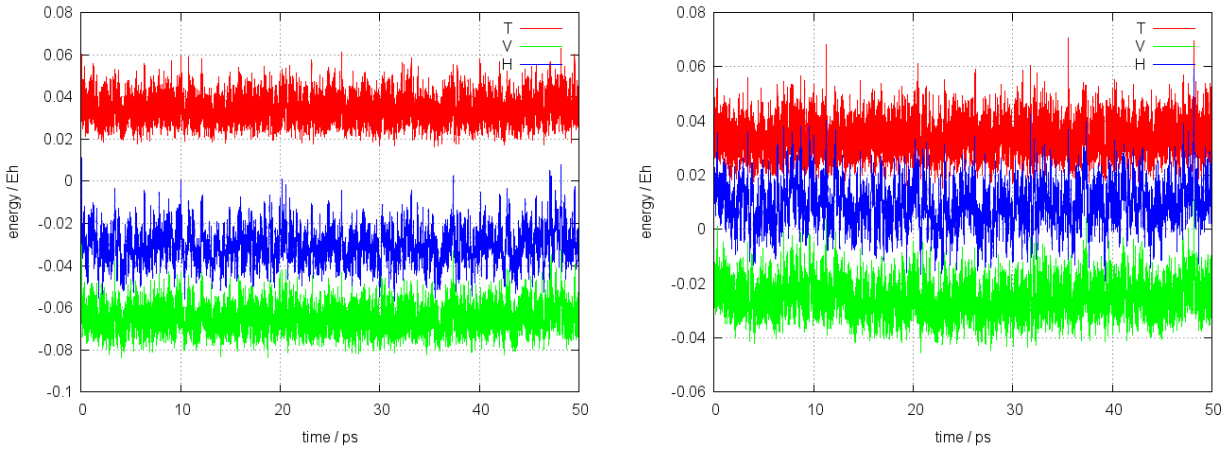

Figure SM.1. The kinetic (red), potential (green), and total (blue) energies properties monitored along the Brownian dynamics.

t–1DAS@Au

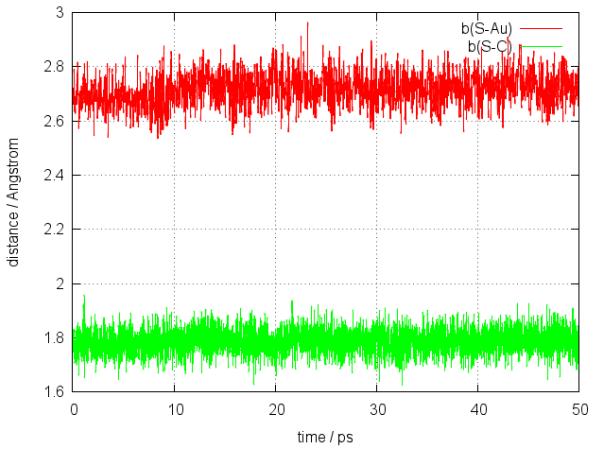

c–1DAS@Au

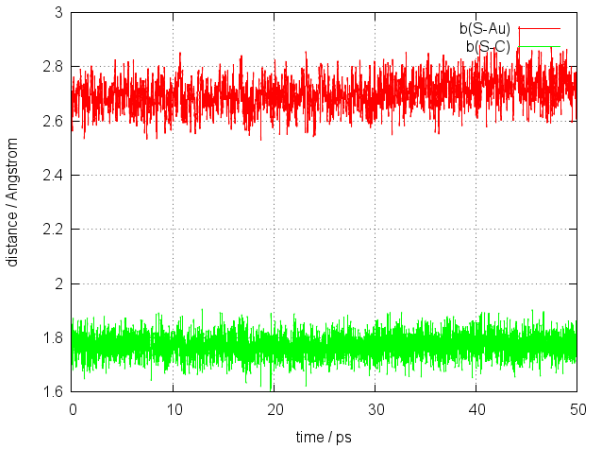

t–1DAS$_2$@Au

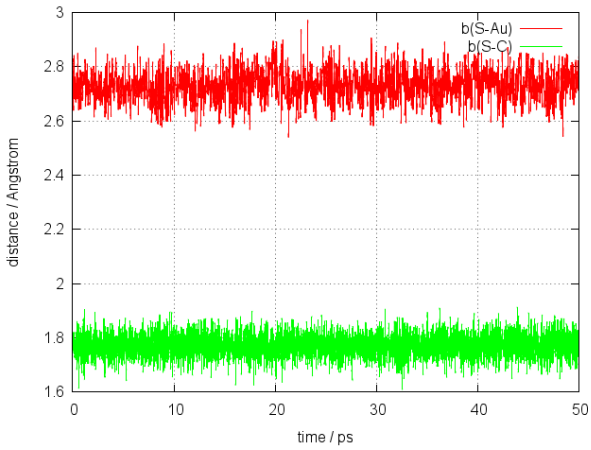

c–1DAS$_2$@Au

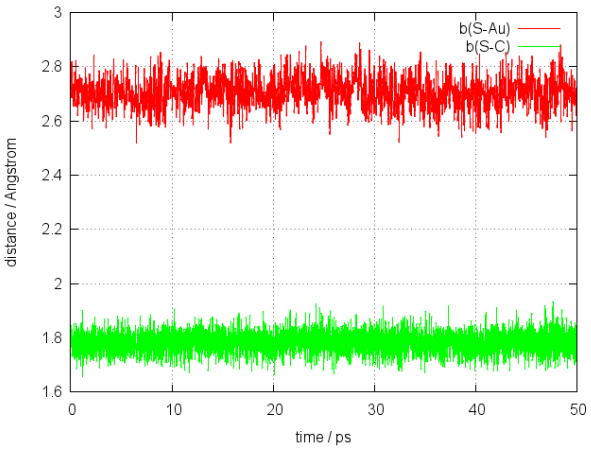

Figure SM.2. The S@Au (red) and S–C (green) bond distances monitored along the Brownian dynamics.

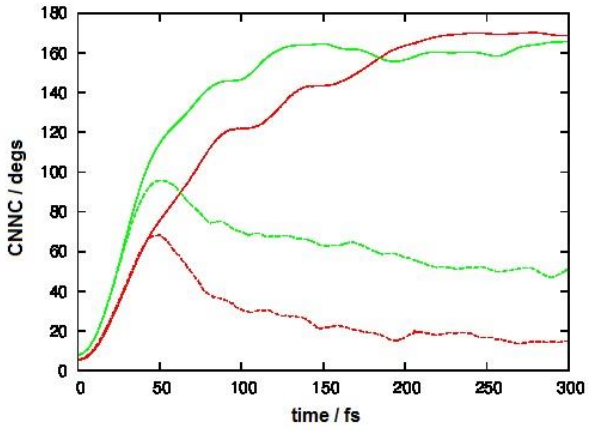

Figure SM.3. Excited state dynamics of *c*–1DAS@Au (red) and *c*–1DAS$_2$@Au (green): CNNC dihedral averaged on reactive (full lines) and unreactive (dashed lines) trajectories.